

Metastable states for an aggregation model with noise

Joep H.M. Evers^{†*} and Theodore Kolokolnikov[†]

[†]*Department of Mathematics and Statistics, Dalhousie University, Halifax, Canada*

^{*}*Department of Mathematics, Simon Fraser University, Burnaby, Canada*

We study the long-time effect of noise on pattern formation for the aggregation model. We consider aggregation kernels that generate patterns consisting of two delta-concentrations. Without noise, there is a one-parameter family of admissible equilibria that consists of two concentrations whose mass is not necessary equal. We show that when a small amount of noise is added, the heavier concentration “leaks” its mass towards the lighter concentration over a very long time scale, eventually resulting in the equilibration of the two masses. We use exponentially small asymptotics to derive the long-time ODE’s that quantify this mass exchange. Our theory is validated using full numerical simulations of the original model – both of the original stochastic particle system and its PDE limit. Our formal computations show that adding noise destroys the degeneracy in equilibrium solution and leads to a unique symmetric steady state.

1. INTRODUCTION

Aggregation is an ubiquitous natural phenomenon that pervades both the animal world and many inanimate physical systems. In the animal kingdom, group formation is observed across all levels from bacterial colonies and insect swarms to complex predator-prey interactions in fish, birds and mammals. Aggregation is also present in physical systems of all scales from the smallest (Bose-Einstein Condensates, DNA buckyball molecules, fluid vortices) to the largest (galaxies). The emergence of group behaviour is often a consequence of individuals (or atoms) following very simple rules, without any external coordination.

One of the simplest models that achieves aggregation is the so-called aggregation model, which has been the subject of intense study in the last two decades; refer to survey papers [1–4] and references therein. Mathematically, this model may be written as a system of ODE’s for n particles

$$\frac{dx_j}{dt} = \frac{1}{n} \sum_{k=1}^n f(x_j - x_k) \quad (1.1)$$

where the pairwise interaction force $f(x)$ is assumed to be the gradient of a radial potential function, $f(x) = -\nabla P(|x|) = -P'(|x|) \frac{x}{|x|}$. The strength of the force $f(x_j - x_k)$ depends only on the distance between the two particles x_j and x_k , and it acts in the direction between these particles. The system (1.1) corresponds to applying the method of steepest descent to determine the minimizer of the pairwise-interaction energy,

$$E = \sum_{k,j} P(|x_j - x_k|).$$

To get confinement, it is further assumed that the particles repel each other at short distances and attract each other at longer distances (see also [5–7]). In many cases this leads to the formation of swarms. The assumption of long-range attraction and short-range repulsion corresponds to $P(r)$ having a minimum at $r > r_0$ so particles at a distance less than r_0 are attracted to each-other and those at distance bigger than r_0 are repelling. These simple assumptions can give rise to surprisingly complex steady states [8–16] including “soccer balls” in two and three dimensions [8, 9, 13, 14] as well as steady states concentrating on points, curves and surfaces [13–17]. Of particular importance for the dimensionality of the steady state is the strength of repulsion near the origin [8, 9, 14]. For this paper, we focus on the simplest case, where the steady state concentrates on a finite number of points (delta-concentrations), which can occur when the repulsion is sufficiently weak at the origin.

In this work we are interested in how the noise that is inherently present in most of the physical systems can affect the resulting steady state. That is, we consider the model (1.1) with noise, so that (1.1) is replaced by stochastic ODE’s

$$dx_j = \frac{1}{n} \sum_{k=1}^n f(x_j - x_k) dt + \sigma \sqrt{dt} \mathcal{N}_j; \quad (1.2)$$

here $\sigma \sqrt{dt} \mathcal{N}_j$ is the standard Weiner process walk with standard deviation σ^2 ; \mathcal{N}_j denotes the standard normal distribution of mean zero and variance 1. In the continuum limit as the number of particles $n \rightarrow \infty$, the average

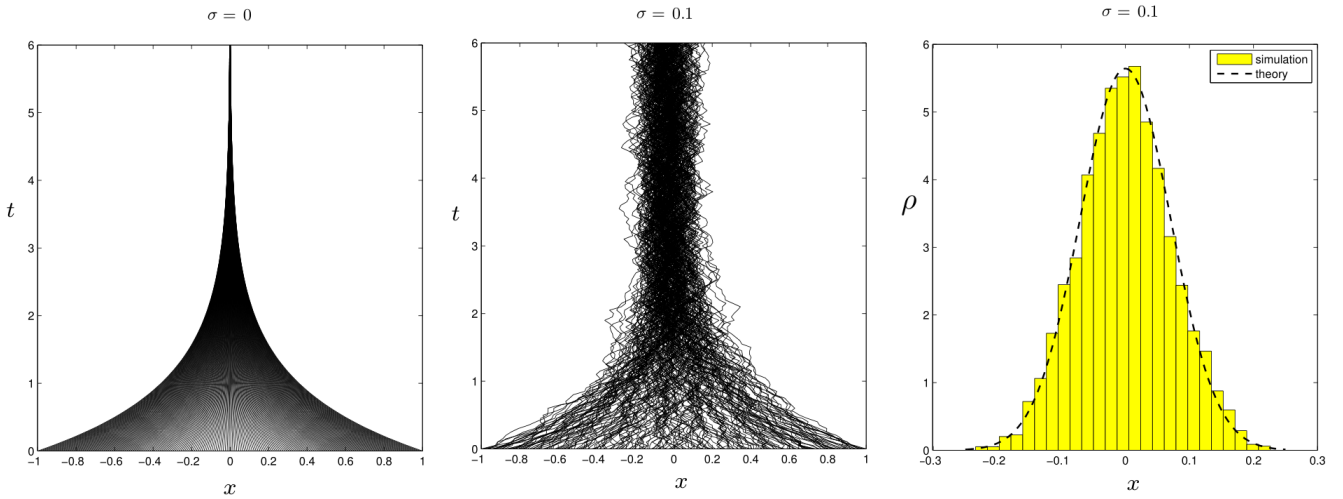


FIG. 1. Left: Particle simulation of deterministic system (1.1) with $f(x) = -x$. Initial conditions consist of $n = 200$ particles equally spaced from each-other. Particles collapse into a single delta-concentration. Middle: Same ODE system but with noise added (1.2). The delta-concentration is “diffused” into a Gaussian. Right: Particle density distribution from the simulation in the middle panel, averaged over 100 time-steps with $t = 10$. The dashed line is the predicted Gaussian profile given by (1.5).

particle density distribution ρ is well approximated by the PDE [3],

$$\rho_t + \nabla \cdot (v\rho) = \varepsilon^2 \Delta \rho, \quad v = \int f(x-y) \rho(y) dy. \quad (1.3)$$

where $\varepsilon^2 = \sigma^2/2$. Equation (1.3) is the starting point for this paper.

The presence of noise can have a profound effect on the steady state, especially if the steady state consists of point concentrations which can be the case when the repulsion is sufficiently weak at the origin [18]. As a motivating example, consider the simplest case,

$$f(x) = -x. \quad (1.4)$$

This corresponds to a potential $P(r) = r^2/2$ that is purely attractive, and is only weakly attractive at the origin (i.e. $P'(0) = 0$). Figure 1 shows the resulting one-dimensional simulations with and without noise for the discrete system (1.2), as well as the associated average density in the presence of noise – computed by averaging the steady state for the last 100 steps of the numerical simulation of (1.2) (for simplicity, we used forward Euler method for these simulations). Without noise, the particle density collapses to a single point (delta function). On the other hand, the noise “diffuses” the delta function and the resulting average steady state density is a Gaussian,

$$\rho(x) = \frac{1}{\sqrt{2\pi\varepsilon^2}} \exp\left(-\frac{x^2}{2\varepsilon^2}\right). \quad (1.5)$$

as was already observed in [18]. Indeed, the steady state satisfies $(v\rho)_x = \varepsilon^2 \rho_{xx}$ where $v(x) = \int - (x-y) \rho(y) dy = -x$, where we assumed that ρ has total mass $M = 1$ and its centre of mass is 0. Integrating once we get the ODE $\varepsilon^2 \rho_x = -x\rho$ whose solution is given by (1.5).

In this paper, we are interested in the effect of small amount of diffusion when the steady steady state consists of more than one delta function. This occurs when repulsion is present (so that the particles do not all collapse into a single point), but the repulsion is sufficiently weak so that far-field attraction causes “clumping” into two or more delta-concentrations. As was shown in [15] in one dimension, (and extended in [13] to two and three dimensions), the necessary condition for this to happen is that $P'(0) = 0$, or equivalently, $f(x) \sim cx$ as $x \rightarrow 0$ for some *positive* constant $c > 0$. To illustrate this phenomenon as well as the results of the paper, consider the simplest such case, namely the double-well potential, $P(r) = -x^2/2 + x^4/4$, so that

$$f(x) = x - x^3. \quad (1.6)$$

Figure 2(left) illustrates the behaviour of the deterministic system (1.1) with $n = 200$ particles, starting with initial conditions consisting of 80 particles near $x = -0.5$ and 120 particles near $x = 0.5$. After some transient time,

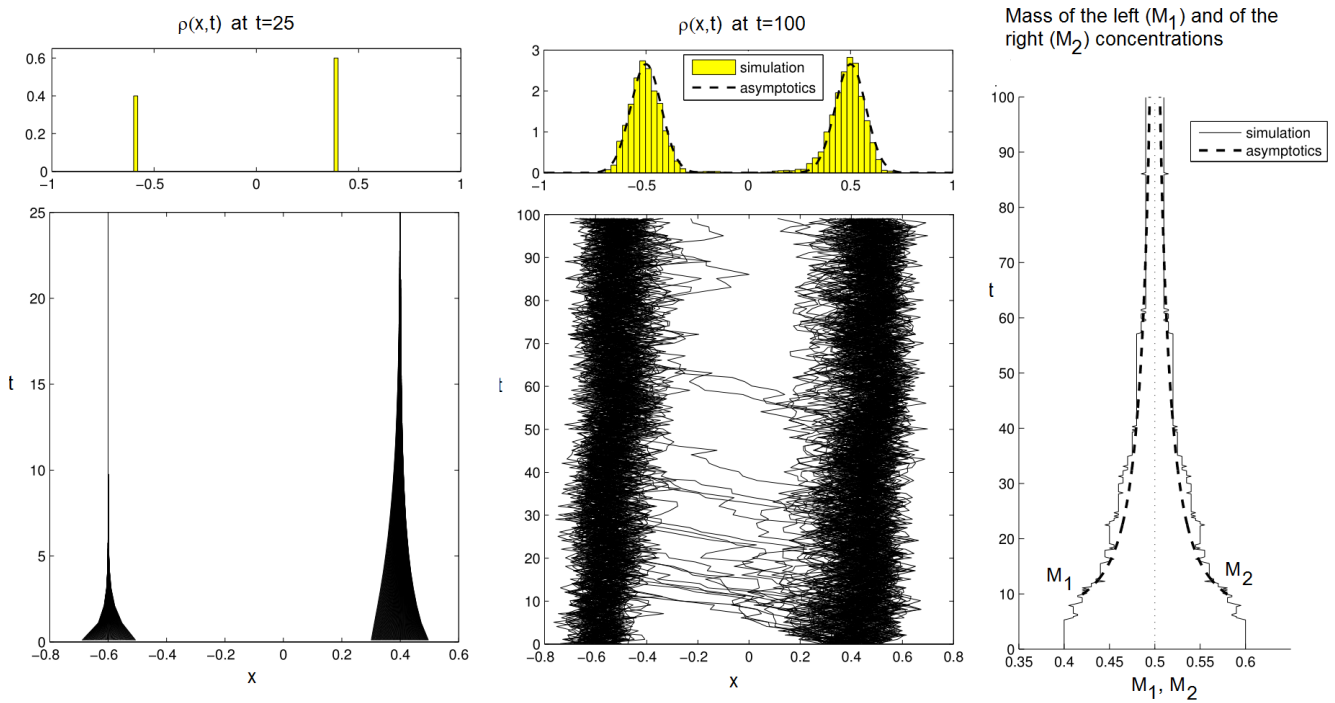


FIG. 2. LEFT: Simulation of the deterministic system (1.1) with $f(x) = x - x^3$. Initial conditions consist 80 particles near $x = -0.5$ and 120 particles near $x = 0.5$ (corresponding to $M_1 = 0.4, M_2 = 0.6$). The long-time dynamics approach two unequal delta-concentrations. The insert in top-left shows the histogram of the final steady state. MIDDLE: Same as left figure, but with $\sigma = 0.075$ noise added. The concentration at the right initially has a larger mass, and it very slowly leaks its mass towards a lighter concentration on the left. RIGHT: The total mass of left and right concentrations of the simulation in the middle is plotted. After a short transient period, a slow mass exchange is apparent, with the two masses gradually equilibrating. Dashed line denotes the asymptotic prediction given by (1.5). The dashed curve is the asymptotic prediction.

the system evolves into a steady state consisting of two delta concentrations, with 40% of the mass at the left concentration and 60% at the right. The distance between the two concentrations is $x = 1$ corresponding to the root of (1.6), and this is trivially seen to be a steady state of (1.1) since $f(0) = f(1) = 0$. Moreover, as was shown in [13, 15], such steady state is actually stable.

Now suppose there is a small amount of noise present in the system (say $\sigma = 0.075$) while keeping all other parameters and initial conditions as in Figure 2(left). The result is shown in Figure 2(middle and right). Initially, the system quickly settles to a two-concentration asymmetric steady state with roughly 40% of mass on the left and 60% of mass on the right, except that the noise “diffuses” the delta concentrations, so that the particles constantly jiggle around, and the average density is a Gaussian. However on a much longer time-scale, there is a very slow exchange of mass that takes place between the left and right concentrations, so that the bigger concentration slowly leaks its mass towards the smaller, until the two concentrations eventually equilibrate. In other words, adding even a small amount of noise eventually “symmetrizes” the asymmetric steady state over a long time. Quantifying this very slow exchange of mass is the goal of this paper.

There are similarities between our work and [19]. They consider the combination of interactions and diffusion on a one-dimensional interval with periodic boundary conditions. Their main focus is on the $O(1)$ stability of steady states consisting of multiple peaks. By contrast, here we are interested in the slow-time evolution (metastability) of these states. We will illustrate our result now.

Our main finding describes the exchange of mass between two asymmetric “diffused” concentrations. The precise statement, for a general kernel $f(x)$, is given in Proposition 3.1. To illustrate the result, consider the cubic kernel (1.6), refer to Figure 2. Starting with arbitrary initial conditions, the system converges, on an $O(1)$ timescale, to a solution consisting of two concentrations. These concentrations will in general have unequal masses (that depend on initial conditions), and their asymptotic profile is a Gaussian spike whose variance depends on their relative masses M_1, M_2 . Once these spikes form, there is a very slow equilibration process, whereby the mass of a heavier spike leaks towards the lighter one. This process is meta-stable, meaning that it takes an exponentially long time (in ε) for the masses to equilibrate. Specializing Proposition 3.1 to (1.6), this slow mass exchange is described

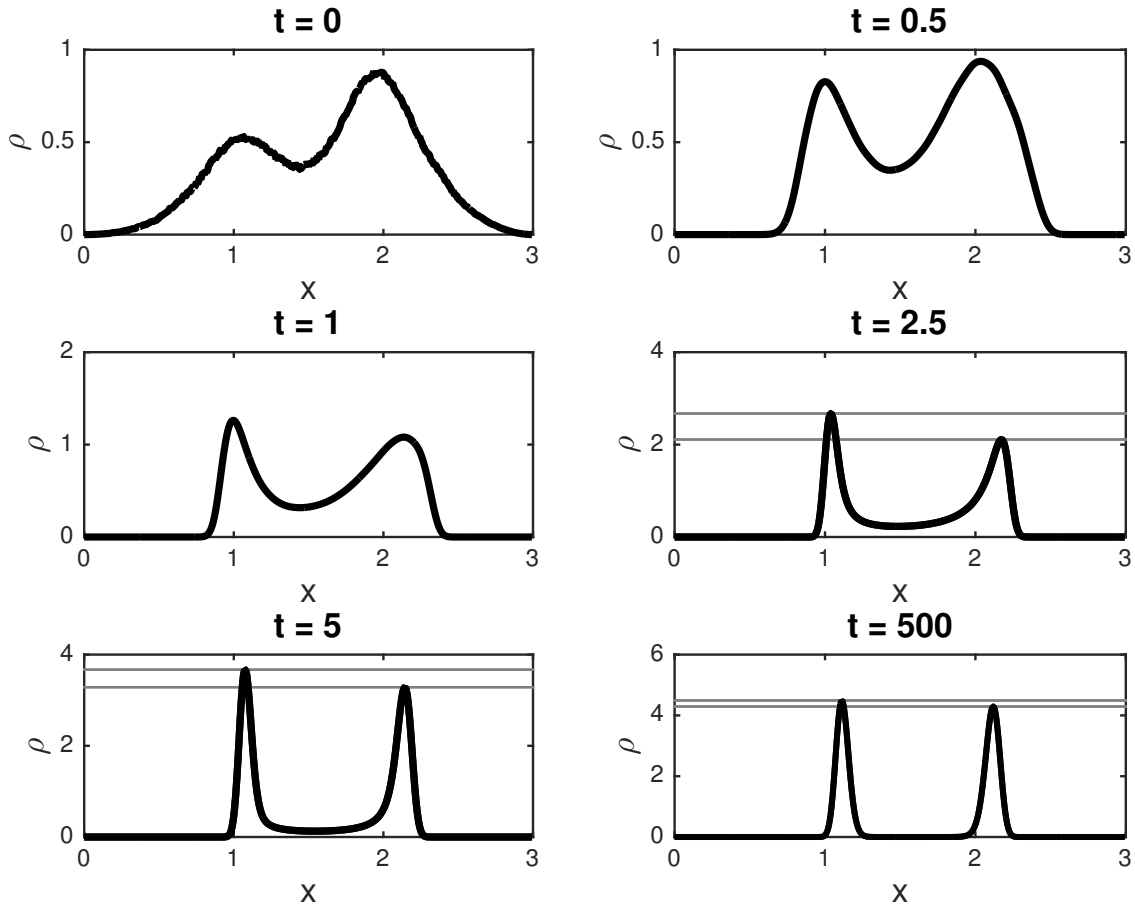


FIG. 3. Evolution of the density profile, for $f(x) = x(1 - x^2)$ and $\varepsilon^2 = 0.001$. In the last three plots, the narrow grey lines indicate the heights of the two maxima. Their heights converge at a slow timescale.

asymptotically by an ODE

$$\frac{d}{dt}M_1 = F(M_1, M_2) - F(M_2, M_1); \quad M_1 + M_2 = M \quad (1.7a)$$

where M is the total mass, M_1 and M_2 are the masses of the two spikes, and

$$F(M_1, M_2) = \frac{M_2}{2\pi} \sqrt{\frac{(2M_2 - M_1)}{M}} (2M_1 - M_2) \exp\left(\frac{-M_2 (2M_1 - M_2)^3}{4M^3 \varepsilon^2}\right). \quad (1.7b)$$

The summary of the paper is as follows. In §2 we construct asymptotically the quasi-steady state consisting of two Gaussians of masses M_1, M_2 . In §3 we derive the equations of mass exchange between M_1 and M_2 , on an exponentially slow timescale, culminating in Proposition 3.1 which is the main result of this paper. From the equations for mass exchange, we show that the masses equilibrate on a long time scale, that is, $M_1 = M_2$ is the unique global steady state of the long-time dynamics. We compare the full numerical solution of the original aggregation-diffusion PDE, to the solutions of a PDE with a simplified velocity and of the ODE, for several values of ε . We conclude with some remarks in §4.

2. QUASI-STEADY STATE

In [13, 15] the authors constructed a steady state of (1.3) with zero diffusion consisting of discrete number ($N \geq 2$) of delta-concentrations. This happens when $f(x)$ is linear near the origin, such as for example (1.6). More generally,

we will assume that:

$$\begin{cases} f(x) \text{ is odd;} \\ f(x) \text{ has a positive root at } x = a; \\ f(x) \text{ is } C^1 \text{ at } x = 0 \text{ and } x = a \text{ with } f'(0) > 0 \text{ and } f'(a) < 0. \end{cases} \quad (2.8)$$

Under these assumptions, a two-delta steady state of (1.3) with $\varepsilon = 0$ has the form

$$\rho(x, t) \sim M_1 \delta(x - x_1) + M_2 \delta(x - x_2) \text{ with } x_2 - x_1 = a, \quad M_1 + M_2 = M \quad (2.9)$$

where M is the total mass. Upon substituting (2.9) into $v = f * \rho$ we obtain that

$$v(x) = M_1 f(x - x_1) + M_2 f(x - x_2) \quad (2.10)$$

Turning on ε in (1.3) “diffuses” the delta concentrations, so that the $\delta(x - x_1)$ is replaced by a “spike” that has width of $O(\varepsilon)$. That is, we write

$$\rho(x, t) \sim M_1 \frac{1}{\varepsilon} w_1 \left(\frac{x - x_1}{\varepsilon} \right) + M_2 \frac{1}{\varepsilon} w_2 \left(\frac{x - x_1}{\varepsilon} \right) \quad (2.11)$$

where $w_i(y)$ is the spike profile that is to be computed, with $\int_{-\infty}^{\infty} w_i(y) dy = 1$ and $w_i(y) > 0$ for all y . Substituting (2.11) into $v = f * \rho$, and expanding the resulting integral in terms of Taylor series, we find that the leading-order expression for the velocity v is then still given by (2.10) up to $O(\varepsilon)$ order. To compute the profile of the left spike $w_1(y)$, we let $x = x_1 + \varepsilon y$ and expand (2.11). We have $v(x_1) = 0$ so that

$$v(x_1 + \varepsilon y) \sim -\varepsilon c_1 y, \quad c_1 = -v'(x_1) \sim -(M_1 f'(0) + M_2 f'(a)). \quad (2.12)$$

We then substitute (2.12) into the steady state equation after discarding ρ_t (this is the assumption that ρ is a quasi-state). Near $x = x_1 + \varepsilon y$ we then obtain, up to exponentially small terms,

$$(yc_1 w_1)_y \sim w_{1yy}.$$

Assuming decay as $y \rightarrow \pm\infty$ yields

$$yc_1 w_1 + w_{1y} \sim 0$$

so that

$$w_1 \sim \frac{1}{\sqrt{2c_1\pi}} \exp\left(\frac{-y^2}{2} c_1\right). \quad (2.13)$$

A necessary condition for decay is that $c_1 > 0$. Performing a similar computation for w_2 we obtain the following result.

Proposition 2.1. *Suppose that $f(x)$ satisfies conditions (2.8) and suppose that M_1, M_2 satisfy*

$$-f'(0)/f'(a) < M_1/M_2 < -f'(a)/f'(0). \quad (2.14)$$

Then (1.3) admits a quasi-equilibrium steady state that has the form

$$\rho(x, t) \sim \sum_{j=1}^2 \frac{M_j}{\varepsilon} \sqrt{\frac{2}{\pi c_j}} \exp\left(-\left(\frac{x - x_j}{\varepsilon}\right)^2 \frac{c_j}{2}\right) \quad (2.15)$$

with $x_2 - x_1 = a$ and $c_j = -v'(x_j)$ with v given by (2.10); that is

$$c_1 = -(M_1 f'(0) + M_2 f'(a)); \quad c_2 = -(M_2 f'(0) + M_1 f'(a)). \quad (2.16)$$

The masses M_1, M_2 satisfy $M_1 + M_2 = M$ where M is the total mass that is determined by the initial conditions, $M = \int_{-\infty}^{\infty} \rho(x, 0) dx$.

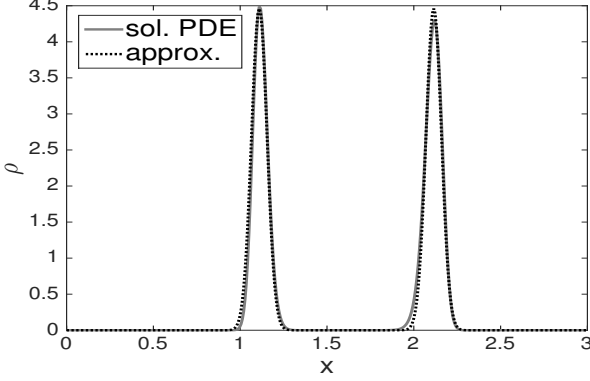


FIG. 4. Density profile at $t = 500$, for $f(x) = x(1 - x^2)$ and $\varepsilon^2 = 0.001$; cf. Figure 3. Superimposed is the approximation (2.15) with $M_1 = M_2$.

As we show in §3, the masses M_1 and M_2 evolve on a timescale much larger than the timescale at which this two-spike profile forms. In Figure 4 we compare the long-time solution of (1.3), as shown in the bottom right of Figure 3, to the approximation (2.15) with $M_1 = M_2$.

Proposition 2.1 generalizes naturally to n concentrations. In this case, the sum $\sum_{j=1}^2$ in (2.15) is replaced by $\sum_{j=1}^n$, with

$$c_j = - \sum_{k=1}^n M_k f'(x_j - x_k). \quad (2.17)$$

and the condition $x_2 - x_1 = a$ is replaced by a system

$$\sum_{k=1}^n M_k f(x_j - x_k) = 0, \quad j = 1 \dots n. \quad (2.18)$$

Finally, the two conditions (2.14) are replaced by n conditions

$$\sum_{k=1}^n M_k f'(x_j - x_k) < 0. \quad (2.19)$$

3. METASTABLE DYNAMICS

We now derive the ODE describing the slow-time dynamics for the mass exchange between M_1 and M_2 . The starting point is the PDE (1.3) with v as given by (2.10). Note from the expansion for v near x_1 (2.12) that $v(x_1) = 0$ and $v'(x_1) < 0$ (which implies that the concentration at $x = x_1$ attracts nearby points). Similarly $v(x_2) = 0$ and $v'(x_2) < 0$. By continuity of $v(x)$, there must be a point \hat{x} such that

$$\hat{x} : \quad \hat{x} \in (x_1, x_2) \text{ with } v(\hat{x}) = 0 \text{ where } v \text{ is given by (2.10)} \quad (3.20)$$

with v increasing at \hat{x} . We further make the following technical assumption which will be needed for global stability:

$$\text{The solution to (3.20) is unique with } v'(\hat{x}) > 0. \quad (3.21)$$

This holds for a large class of functions and in particular if $f'''(x) < 0$ for all $x \in (0, a)$. We identify this point \hat{x} as the boundary point between mass belonging to spike #1 and mass belonging to spike #2.

Assuming that the density decays away from the x_j , we have

$$M_1 \sim \int_{-\infty}^{\hat{x}} \rho(x) dx; \quad M_2 \sim \int_{\hat{x}}^{\infty} \rho(x) dx. \quad (3.22)$$

Integrating (1.3) we therefore obtain

$$\frac{d}{dt}M_1 = \varepsilon^2 \rho_x(\hat{x}), \quad \frac{d}{dt}M_2 = -\varepsilon^2 \rho_x(\hat{x}) \quad (3.23)$$

where we assumed that $\rho \rightarrow 0$ as $x \rightarrow \pm\infty$. We assume that the dynamics are sufficiently slow such that ρ_t term can be discarded in (1.3). Then integrating the resulting ODE we obtain

$$\rho v = \varepsilon^2 \rho_x - \varepsilon^2 \rho_x(\hat{x}), \quad x \in (x_1, x_2), \quad (3.24)$$

where we use that $v(\hat{x}) = 0$.

The solution to (3.24) is given by

$$\rho(x) = \left[\rho(\hat{x}) + \rho_x(\hat{x}) \int_{\hat{x}}^x \exp(-V(z)/\varepsilon^2) dz \right] \exp(V(x)/\varepsilon^2), \quad (3.25)$$

where

$$V(x) = \int_{\hat{x}}^x v(x) dx.$$

Note that $-V(x)$ has a global maximum at $x = \hat{x}$ (by (3.20) and (3.21)), so that we may use Laplace's method to evaluate the integral in (3.25). We obtain:

$$\int_{\hat{x}}^x \exp(-V(z)/\varepsilon^2) dz \sim \text{sign}(x - \hat{x}) \varepsilon \sqrt{\frac{\pi}{2v'(\hat{x})}}, \quad |x - \hat{x}| \gg O(\varepsilon)$$

To determine $\rho_x(\hat{x})$, let $x \rightarrow x_i$, $i = 1, 2$, and match (3.25) with the inner solution as given by (2.15). Expanding near x_j , we let $x = x_j + \varepsilon y$ and expand

$$\begin{aligned} V(x_j + \varepsilon y) &= \int_{\hat{x}}^{x_j} v(s) ds + v(x_j) \varepsilon y + v'(x_j) \varepsilon^2 \frac{y^2}{2} + \dots \\ &\sim \int_{\hat{x}}^{x_j} v(s) ds - c_j \varepsilon^2 \frac{y^2}{2} \end{aligned}$$

where $c_j = -v'(x_j)$ is as given in (2.16). Therefore the outer region written in inner variables near x_j becomes

$$\rho(x_j + \varepsilon y) \sim \left[\rho(\hat{x}) + \text{sign}(x_j - \hat{x}) \rho_x(\hat{x}) \varepsilon \sqrt{\frac{\pi}{2v'(\hat{x})}} \right] \exp \left(\frac{1}{\varepsilon^2} \int_{\hat{x}}^{x_j} v(s) ds \right) \exp \left(-c_j \frac{y^2}{2} \right). \quad (3.26)$$

On the other hand, the inner region near $x = x_j + \varepsilon y$ as derived in (2.15) is

$$\rho \sim \frac{M_j}{\varepsilon} \sqrt{\frac{2}{\pi c_j}} \exp \left(-c_j \frac{y^2}{2} \right). \quad (3.27)$$

Matching (3.27) and (3.26) yields

$$\frac{M_1}{\varepsilon} \sqrt{\frac{2}{\pi c_1}} = \left[\rho(\hat{x}) - \rho_x(\hat{x}) \varepsilon \sqrt{\frac{\pi}{2v'(\hat{x})}} \right] \exp \left(\frac{1}{\varepsilon^2} \int_{\hat{x}}^{x_1} v(s) ds \right), \quad (3.28a)$$

$$\frac{M_2}{\varepsilon} \sqrt{\frac{2}{\pi c_2}} = \left[\rho(\hat{x}) + \rho_x(\hat{x}) \varepsilon \sqrt{\frac{\pi}{2v'(\hat{x})}} \right] \exp \left(\frac{1}{\varepsilon^2} \int_{\hat{x}}^{x_2} v(s) ds \right). \quad (3.28b)$$

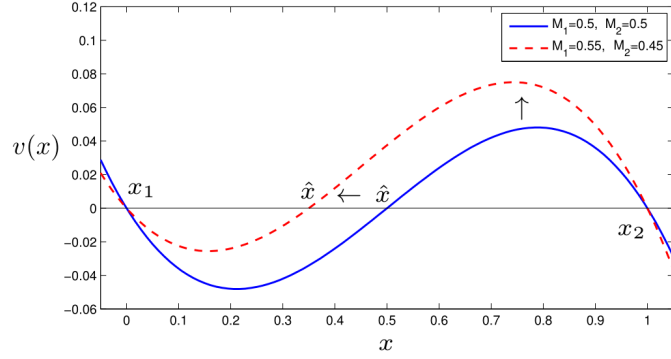


FIG. 5. The graph of $v(x) = M_1 f(x) + M_2 f(x-1)$ with $f(x) = x - x^3$ and with M_1, M_2 as indicated in the legend. Increasing M_1 moves \hat{x} to the left.

Solving for $\rho_x(\hat{x})$ from (3.28) and then using (3.23) finally yields

$$\frac{dM_1}{dt} \sim M_2 \sqrt{\frac{v'(\hat{x})}{\pi^2 c_2}} \exp\left(-\frac{1}{\varepsilon^2} \int_{\hat{x}}^{x_2} v(s) ds\right) - M_1 \sqrt{\frac{v'(\hat{x})}{\pi^2 c_1}} \exp\left(-\frac{1}{\varepsilon^2} \int_{\hat{x}}^{x_1} v(s) ds\right); \quad (3.29a)$$

$$\frac{dM_2}{dt} = -\frac{dM_1}{dt}. \quad (3.29b)$$

It is clear that the symmetric configuration $M_1 = M_2$ is an equilibrium of the ODE (3.29), since in this case, $\hat{x} = x_1 + a/2$ and $c_1 = c_2$, $\int_{\hat{x}}^{x_1} v(s) ds = \int_{\hat{x}}^{x_2} v(s) ds$. We now show that it is indeed a global attractor, provided (3.21) holds. From the equation $v(x) = M_1 f(x - x_1) + M_2 f(x - x_2)$ and the fact that $f(x - x_1)$ is positive for $x \in (x_1, x_2)$, it follows that $v(x)$ is an increasing function of M_1 . This in turn shows that \hat{x} is a decreasing with M_1 , $\int_{\hat{x}}^{x_1} v(s) ds$ is decreasing with M_1 and $\int_{\hat{x}}^{x_2} v(s) ds$ is increasing with M_1 . Refer to Figure 5. It then follows from (3.29) that $\frac{dM_1}{dt} < 0$ whenever $M_1 > M_2$ and $\frac{dM_1}{dt} > 0$ when $M_1 < M_2$. This shows that any admissible initial masses satisfying (2.14) evolve towards the equal-mass $M_1 = M_2$ configuration.

We now summarize.

Proposition 3.1. *Consider the quasi-state constructed in Proposition 3.1. The spike masses $M_1(t)$, $M_2(t)$ evolve on an exponentially slow time-scale according to (3.29), where $v(x)$ is given by (2.10) and \hat{x} satisfies (3.20). Moreover, suppose that in addition to properties (2.8), $f(x)$ also satisfies: $f'''(x) < 0$ for $x \in (0, a)$. Then $M_1 = M_2 = M/2$ is the global attractor of (3.29) where $M = M_1 + M_2$ is the total mass, so that $M_1(t), M_2(t) \rightarrow M/2$ as $t \rightarrow \infty$.*

To illustrate Proposition 3.1, take

$$f(x) = x(1 - x^2).$$

Then the right hand side in (3.29) can be computed explicitly. Without loss of generality (translation invariance), assume that $x_1 = 0$, hence $x_2 = 1$ so that $v(x)$ given by (2.10) becomes

$$v(x) = x(1 - x)(M_1 - 2M_2 + M x).$$

The unique $\hat{x} \in (0, 1)$ for which $v(\hat{x}) = 0$ is therefore explicitly given by

$$\hat{x} = \frac{2M_2 - M_1}{M},$$

and we compute

$$v'(\hat{x}) = \frac{(2M_2 - M_1)(2M_1 - M_2)}{M}; \quad (3.30)$$

and

$$\int_{\hat{x}}^{x_1} v(x) dx = \frac{M_1(2M_2 - M_1)^3}{4M^3}; \quad \int_{\hat{x}}^{x_2} v(x) dx = \frac{M_2(2M_1 - M_2)^3}{4M^3}. \quad (3.31)$$

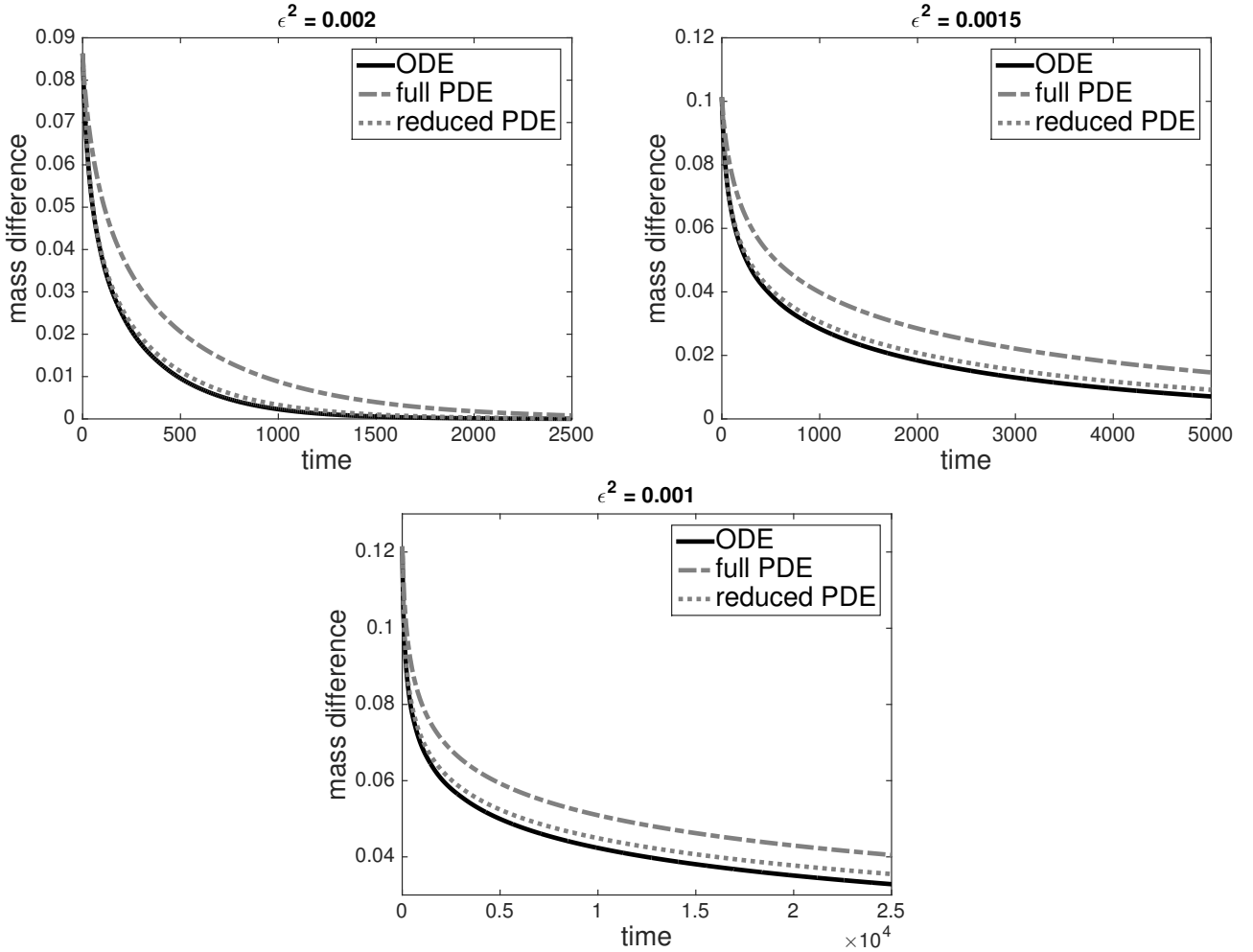


FIG. 6. Mass difference as a function of time, for the full PDE, reduced PDE and ODE. Top left: $\epsilon^2 = 0.002$. Top right: $\epsilon^2 = 0.0015$. Bottom: $\epsilon^2 = 0.001$.

Substituting (3.30) and (3.31) into (3.29) yields an explicit ODE (1.7) for mass exchange dynamics. In Figure 6, we compare the solution to (1.7) with the full numerical solution to the original PDE (1.3). In addition, the dashed plot shows the reduced PDE, where we replace the convolution $v = f * \rho$ by an explicit formula (2.10) for the velocity v when computing the solution to (1.3). The masses M_1 and M_2 in (2.10) were computed numerically using (3.22) for each time-step. In either the full or reduced PDE, we used finite differences with semi-implicit time stepping: $v(x)$ is computed explicitly at each time step, while the update for $\rho(x, t + \Delta t)$ is done implicitly. We verified the accuracy by using several stepsizes. Interestingly, while the ODE (1.7) agrees reasonably well with the full PDE, it agrees even better with the reduced PDE system – which is the starting point for the derivation of Proposition 3.1. This makes sense, since there is a significant error that was made in this reduction. For numerical integration, we took the computational domain to be of size $x \in [0, 3]$. Because of the exponential decay outside the spikes, doubling the domain size did not change the results. The initial conditions were taken to be (2.15), with $M_1 = 0.35$, $M_2 = 0.65$. The centers of the two Gaussian peaks are taken a distance 1 apart. We also waited $t = 10$ time units to let the transients die out before starting the comparison; at $t = 10$ the system already converged to the quasi-steady state.

Figure 6 shows that in general the mass difference that follows from the ODE corresponds well to the solution of the reduced PDE. Both of them deviate from the solution of the full PDE, but they still exhibit the same trend. As ϵ decreases, the equilibration process takes more time, as the effect of the diffusion term is smaller. However, the maximum deviation between the curve for the ODE and the full PDE decreases as ϵ decreases.

4. DISCUSSION

In this paper we focused on the steady states of the aggregation equation with noise (1.3) that consists of two nearly-Dirac concentrations. An important implication of the work presented here, is that not all steady states of the zero-diffusion equation can be recovered as the limit as $\varepsilon \rightarrow 0$ of a sequence of steady states of the aggregation-diffusion equation. This concerns in particular the two-Dirac steady states of unequal mass. Nevertheless, on short timescales some reminiscents of these unequal-mass steady states are still present. To be more precise, there is an intermediate timescale in which a state consisting of two Diracs of unequal mass persists as a metastable state.

We have shown that the process of equilibration can be described asymptotically by an ODE for the evolution of the mass associated to each of the spikes. This ODE is valid on an exponentially long timescale, after the initial two-spike quasi-state profile is formed on an $O(1)$ timescale.

An interesting, but nontrivial complication arises when one wants to derive an ODE for the mass evolution for three or more spikes. In the case of two spikes, these are centred a distance a apart (with a such that $f(a) = 0$). For more than two spikes a delicate balance needs to be satisfied: there is an algebraic system of equations involving the masses and mutual distances, such that the velocity at each centre is zero. This algebraic relation, together with an ODE for the evolution of each mass, accounts for the simultaneous evolution of the centres of the spikes and the masses towards equilibrium.

As in the case of two spikes, the steady state consisting of three delta-concentrations in the absence of diffusion is degenerate: there is an arbitrariness in how the three masses are distributed among the three holes, and there are two degrees of freedom (three masses subject to constraint $M_1 + M_2 + M_3 = 1$). However when the diffusion is turned on, this two-parameter family of steady states should “collapse” into a unique steady state. It would be very interesting to characterize precisely which mass fractions are “selected” by the diffusion. Unlike the two-spike solution where diffusion “chooses” the equal-mass configuration, in the case of the three-spike configuration, the diffusion should in general select unequal mass fractions.

It would be interesting to extend these results to two and higher dimensions. In two dimensions, at least three delta-concentrations are required for stability [13] (in the case three delta-concentrations, their locations form an equilateral triangle). The construction of the inner solution near the spike is analogous to the derivation in §2. On the other hand, the outer region cannot be easily solved, as it requires solving a fully two-dimensional PDE, and performing matching is a nontrivial problem. Nonetheless there is a hope that WKB-type techniques can be used to approximate the solution to the outer region for small diffusion. It would be interesting if similar “equilibration” results can be obtained in two dimensions.

[1] A. Mogilner, L. Edelstein-Keshet, A non-local model for a swarm, *J. Math. Biol.* 38 (1999) 534–570.

[2] C. M. Topaz, A. L. Bertozzi, M. A. Lewis, A nonlocal continuum model for biological aggregation, *Bull. Math. Bio.* 68 (2006) 1601–1623.

[3] D. Morale, V. Capasso, K. Oelschläger, An interacting particle system modelling aggregation behavior: from individuals to populations, *Journal of mathematical biology* 50 (1) (2005) 49–66.

[4] A. J. Bernoff, C. M. Topaz, Nonlocal aggregation models: A primer of swarm equilibria, *SIAM Review* 55 (4) (2013) 709–747.

[5] D. Balagué, J. A. Carrillo, Y. Yao, Confinement for repulsive-attractive kernels, *Discret. Contin. Dyn. S. Ser. B* 19 (2014) 1227–1248.

[6] J. A. Cañizo, J. A. Carrillo, F. S. Patacchini, Existence of compactly supported global minimisers for the interaction energy, *Archive for Rational Mechanics and Analysis* 217 (3) (2015) 1197–1217.

[7] R. Simione, D. Slepčev, I. Topaloglu, Existence of ground states of nonlocal-interaction energies, *J. Stat. Phys.* 159 (2015) 972–986.

[8] T. Kolokolnikov, H. Sun, D. Uminsky, A. L. Bertozzi, Stability of ring patterns arising from two-dimensional particle interactions, *Physical Review E* 84 (1) (2011) 015203.

[9] J. H. Von Brecht, D. Uminsky, T. Kolokolnikov, A. L. Bertozzi, Predicting pattern formation in particle interactions, *Mathematical Models and Methods in Applied Sciences* 22 (supp01) (2012) 1140002.

[10] J. H. von Brecht, D. Uminsky, On soccer balls and linearized inverse statistical mechanics, *Journal of nonlinear science* 22 (6) (2012) 935–959.

[11] R. C. Fetecau, Y. Huang, T. Kolokolnikov, Swarm dynamics and equilibria for a nonlocal aggregation model, *Nonlinearity* 24 (10) (2011) 2681.

[12] A. L. Bertozzi, T. Laurent, F. Léger, Aggregation and spreading via the Newtonian potential: the dynamics of patch solutions, *Mathematical Models and Methods in Applied Sciences* 22 (supp01) (2012) 1140005.

[13] T. Kolokolnikov, Y. Huang, M. Pavlovski, Singular patterns for an aggregation model with a confining potential, *Physica D: Nonlinear Phenomena* 260 (2013) 65–76.

[14] D. Balagué, J. Carrillo, T. Laurent, G. Raoul, Dimensionality of local minimizers of the interaction energy, *Archive for Rational Mechanics and Analysis* 209 (3) (2013) 1055–1088.

- [15] K. Fellner, G. Raoul, Stable stationary states of non-local interaction equations, *Mathematical Models and Methods in Applied Sciences* 20 (12) (2010) 2267–2291.
- [16] J. von Brecht, T. Kolokolnikov, A. L. Bertozzi, H. Sun, Swarming on random graphs, *Journal of Statistical Physics* 151 (1-2) (2013) 150–173.
- [17] E. J. Hackett-Jones, K. A. Landman, K. Fellner, Aggregation patterns from nonlocal interactions: Discrete stochastic and continuum modeling, *Physical Review E* 85 (4) (2012) 041912.
- [18] B. D. Hughes, K. Fellner, Continuum models of cohesive stochastic swarms: the effect of motility on aggregation patterns, *Physica D: Nonlinear Phenomena* 260 (2013) 26–48.
- [19] E. Geigant, M. Stoll, Stability of peak solutions of a non-linear transport equation on the circle, *Electronic Journal of Differential Equations* 2012 (157) (2012) 1–41.